INTERNATIONAL JOURNAL OF
ENERGY AND ENVIRONMENT

Volume 7, Issue 1, 2016 pp.23-36
Journal homepage: www.IJEE.IEEFoundation.org

Experimental and theoretical investigation of the effect of rotating circular cylinder speed on the lift and drag forces

Ghassan F. Smaisim[1,2], Oula M.H. Fatla[1,3], Agustin Valera-Medina[1], A.M. Rageb[4], N. Syred[1]

[1]School of Engineering, Cardiff University, Cardiff, United Kingdom.
[2] College of Engineering, Kufa University, Iraq.
[3] College of Engineering, Al-Qadisya University, Iraq.
[4] College of Engineering, Basrah University, Iraq.

Abstract
Flow past a circular cylinder is a problem for understanding flow around bluff bodies. This flow has been studied both experimentally and numerically of laminar infinite flow of viscous incompressible fluid around a rotating circular cylinder at Reynolds number 80,120,160 and dimensionless rotation rate, α , (ratio of cylinder surface speed to the free stream velocity) varying from 0 to 6 has been carried out. Navier–Stokes and continuity equations were solved numerically by using finite volume technique is conducted with ANSYS CFX 15 package program. High Speed Photography and LDV, present new experimental results for correlation purposes, captured the flow profile. Rotation can be used as a drag reduction technique. Comparison with previous studies showed good agreement.

Keywords: Rotating cylinder; Lift force; Drag force; Experimental visualization; CFD; LDV.

1. Introduction

Many scientific applications have been devoted to the problem of the fluid flow around a rotating cylinder. The parameter to this case is determined by non- dimensional which are Reynolds number Re = $U_\infty d/\nu$= and rotation rate $\alpha = \omega D/2U_\infty$ (where U_∞ is the freestream velocity; d is the cylinder diameter and ν is kinematic viscosity of fluid; and ω is the angular velocity of the cylinder rotation).
Prandtl [1] investigated experimentally this subject, where it was shown that at α≈ 2 the Karman vortex street was depressed and the fluid flow pattern becomes steady. This conclusion conforms to many other experiments Coutanceau and Menard [2], Lam [3] and another numerical investigations Chew et al. [4], Kang et al. [5], Stojkovic et al. [6], Mittal and Kumar [7], Mazo and Morenko [8], Prikhod'ko and Redtchits [9]. Badr et al. [10] studied numerically and experimentally the unsteady two-dimensional flow past a circular cylinder for $103 \leq Re \leq 104$ and $0.5 \leq \alpha \leq 3$. They solved the equations in terms of vorticity and stream function. Ingham & Tang [11] studied a numerical solution of the steady two-dimensional incompressible equations for Re = 60 and 100 and $0 \leq \alpha \leq 1$. They avoid the difficulties regarding the boundary conditions far from the cylinder. Kumar et al. [12] developed the previous work of Mittal & Kumar [7] and studied experimentally the water flow at Reynolds numbers of 200, 300, and 400 and $0 \leq \alpha \leq 5$. They used quantitative measurements using a particle image velocimetry technique

and hydrogen bubble technique to diagnostic flow visualization. They preview a global view of the wake structure at different Reynolds numbers and various rotation rates. Vortex shedding activity is observed to occur from a =0 to α =1.95. Reynolds number is found to have a strong effect on the wake morphology near the suppression rotation rate, α = 1.95. The vortex shedding once more continued at $4.34 < \alpha < 4.70$ as shown previously for Re=200 and the shed vortices are shows as symbol of rotation rates. Al-Maliky [13] investigated numerically laminar flow of incompressible, two-dimensional, and steady state over rotating circular cylinder at rotating rates $1 \leq \alpha \leq 6$ and Re=200,400,800 and 1000 Navier – Stokes and continuity equations were solved numerically by using finite volume technique. Results show an increase of pressure, and skin friction coefficients with increasing of rotation rate at same Reynolds number. Ayyappan & Vengadesan [14] investigated the fluid flow around two rotating cylinders at a constant speed ratio of three and Reynolds number 100 and 500. The momentum injection from the rod is found to alter the flow characteristics behind the main cylinder. They concluded at certain diameter ratio and stagger angle, the vortex shedding behind the main cylinder was suppressed. Pralits et al. [15] presented a linear stability of the flow past a rotating cylinder and studied the onset two-dimensional and three-dimensional bifurcations for Re=40, 50, 60 and 100 at $0 \leq \alpha \leq 5$. They denoted modes at rotation rates $\alpha < 2$ as mode I and modes for higher rates values, $\alpha > 2$, as mode II. They found a reasonable explanation for the difference between numerical and experimental findings existing so far at high rotation rates. The unsteady shedding mode II cannot be observed in experimentally and the stationary three-dimensional solution is unstable for Re below the critical value of two-dimensional instabilities.
The present numerical method at Re=100 and α=0 is validated against the results of [5-7, 14, 16, 17] and an excellent agreement is shown in Table1.

Table 1. Comparison of present numerical results with the published results for Re=100 at α=0

Source	St	C_D	C_L
Kang et al. [5]	0.164	1.34	0.236
Stojkovic´ et al. [6]	0.165	1.34	0.226
Mittal & Kumar [7]	0.164	1.32	0.230
Ayyappan & Vengadesan [14]	0.163	1.39	0.253
Engelman & Jamina [16]	0.170	1.40	0.257
Meneghini et al. [17]	0.165	1.37	0.257
Present work	0.168	1.36	0.245

2. Experimental setup

The experiments for this study were carried out in duct with a test section constructed from Perspex material of clear ACRYLIC (ACRYLITE FF) sheet of depth 0.15 m, length 1.2 m, and width 1.2 m of 10mm thick. Centrifugal fan with impeller diameter (500mm) used to suction the air from the test section. The centrifugal fan was drive by an electric motor of (3 hp) with (3000 r.p.m). The air velocity needed to achieve maximum Reynolds number of 160 was 0.195m/s in the present experiments. The measurements were performed in the middle of the test section, see Figure 1.
The cylinder used in the experiments are given in our earlier work [18] which is stainless steel rod of length 150mm and diameter 1.2 mm so that the ratio of the height duct to the diameter of the cylinder H/D=100. The cylinder, with bearing sleeve at two ends, was mounted on a fixture. The circular cylinder was rotated with belt, pulley and motor arrangement. A pulley was fixing by a bolt on the cylinder to rotate it different values of speed by V-belt that connect to three-phase motor MT63B14-2. The motor was controlled by Adjustable Speed Drive type Simovert, model P6SE1005-3AA21. The rotation rate of the cylinder was monitored by a Digital Photo/Contact Tachometer model DT-2236 from Lutron Electronic Enterprise CO., LTD. Laser Doppler Velocimetry (LDV) used of a 543-TSI-A01 system and a PDM 1000 model processor to examine the turbulence intensity and velocity profiles. Prosound GT-800 Fog Smoke Machine with output power of the heater 800W was utilized as fog generator to scatter particles, as the densities of the smoke and air were enough that allow excellent particles suspension. A 450500 model probe was calibrated at the horizontal to reduce the dispersion of the laser beams by the bearing and the bearing house. It was mounted on a traverse mechanism. Measuring volume was located at 30 mm height from the cylinder. Ten measurement points obtained for all cases spaced at 10mm between each other, Figure 2. Results were analyzed using the FlowSizer software. Flow turbulence was also characterized using the LDV data. A PhotronFastcam High Speed Camera with model APX RS of 250,000 frames/sec maximum speed velocity was used also. In order to increase the visual

field and to avoid any resolution problem, the camera was setup at only 700 fps. The camera was positioned at 1000 mm from the cylinder. The images were analyzed using the PFV 531 software. Similarly to the LDV, smoke was also used to provide insights of the flow paths.

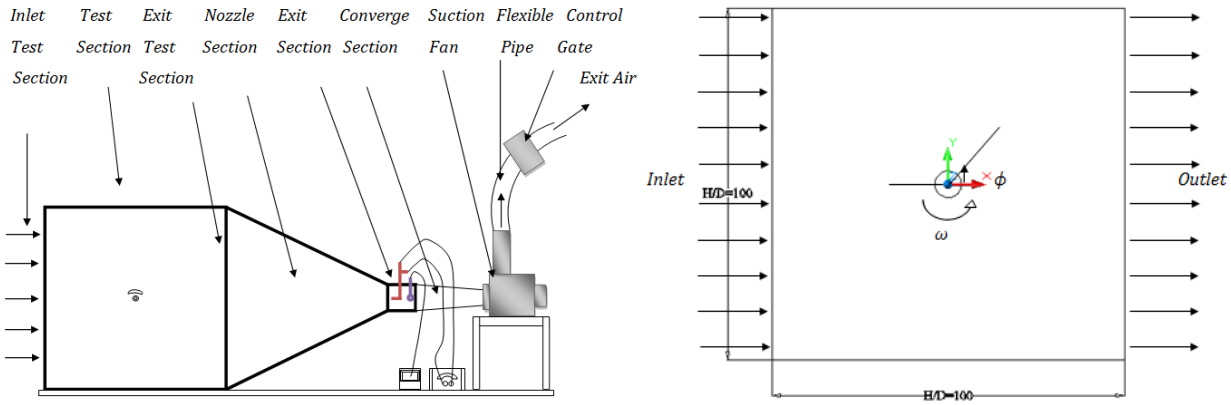

Figure 1. Schematic of the (a) airflow rate system schematic (b) test section dimension

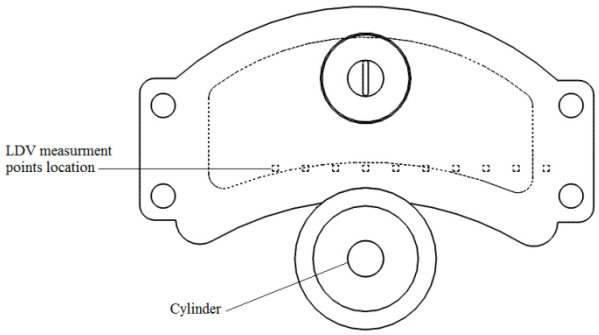

Figure 2. LDV measurement points [18]

3. Numerical analysis

3.1 Governing equation and boundary conditions

The governing equations used in this study based on steady, three-dimensional, laminar flow and incompressible. The momentum field subjected to Dirichlet no-slip boundary conditions at the duct wall and the cylinder wall. The thermo physical properties of the fluid are constant. At the inlet of the flow, the velocities were adjusted to cover needed Reynolds numbers and the outlet condition as the zero pressure gauge. General continuity, momentum equations for Cartesian coordinates system are:

$$\frac{\partial u}{\partial x}+\frac{\partial v}{\partial y}+\frac{\partial w}{\partial z}=0 \tag{1}$$

$$\rho\left(u\frac{\partial u}{\partial x}+v\frac{\partial u}{\partial y}+w\frac{\partial u}{\partial z}\right)=-\frac{\partial p}{\partial x}+\mu\left(\frac{\partial^2 u}{\partial x^2}+\frac{\partial^2 u}{\partial y^2}+\frac{\partial^2 u}{\partial z^2}\right) \tag{2}$$

$$\rho\left(u\frac{\partial v}{\partial x}+v\frac{\partial v}{\partial y}+w\frac{\partial v}{\partial z}\right)=-\frac{\partial p}{\partial y}+\mu\left(\frac{\partial^2 v}{\partial x^2}+\frac{\partial^2 v}{\partial y^2}+\frac{\partial^2 v}{\partial z^2}\right) \tag{3}$$

$$\rho\left(u\frac{\partial w}{\partial x}+v\frac{\partial w}{\partial y}+w\frac{\partial w}{\partial z}\right)=-\frac{\partial p}{\partial z}+\mu\left(\frac{\partial^2 w}{\partial x^2}+\frac{\partial^2 w}{\partial y^2}+\frac{\partial^2 w}{\partial z^2}\right) \tag{4}$$

3.2 Numerical method

Flow simulation performed using ANSYS CFX 15 code. The way of checking whether the solution is grid independent or not is to create a grid with more cells to compare the solutions. For 2D cases, grid refinement tests indicate that a grid size of approximately 44500 triangular elements to provide sufficient

accuracy and resolution. For 3D case with full scale geometry the test of the resolution are repeated, and the grid refinement tests indicate that a grid size of approximately 1050000 tetrahedral elements. They provide sufficient accuracy and resolution. The Simple Implicit Method for Pressure-Linked Equations (SIMPLE) was used in order to attain mass conservation and to avoid pressure-velocity decoupling. A convergence criteria of 10^{-6} was used for all residuals to achieve the purpose of convergence acceleration.

4. Results and discussion

4.1 CFD streamline patterns

The fluid flow pattern is shown by streamlines near the cylinder as shown in fig.3 for Re=80, 120 and 160. Similar results to those obtained from [18]. The streamlines for a stationary cylinder show two vortices as a twin-vortex (top clockwise and bottom counterclockwise) behind the cylinder at Re=80 whose size increases at Re=120 and 160 respectively. The flow is symmetric across the stream wise axis of stationary circular cylinder. As the cylinder starts to rotate, the flow becomes asymmetric under the influence of cylinder counterclockwise rotation due to the interaction between the flow generated close to the cylinder and the free-stream flow for rotation speed ratio α=1,2,3,4,5 and 6 for Re=80,120 and 160 respectively as shown in Figure 3. It can be noted that the stagnation point lies on top of the cylinder. As the dimensionless peripheral speed at the surface of the cylinder increases, for a fixed Re, the region of close streamlines around the cylinder extends far from the wall and, as a result, the stagnation point moves upwards of the cylinder. As the rotational speed increases, the region of close streamlines turn into narrow and the stagnation point lies close to the upper surface of the cylinder.

At $\alpha \geq 3$ for all Reynolds number considered, the clockwise-detached vortex disappears by merging into the stream and the flow contains only enveloping vortex with stream structure as it shown at α=6. Thus, at low rotational speed rate α, the flow pattern near the cylinder is strongly affected by viscous forces while at high values of rotational speed the flow is dominated by inertia effect.

Experimentally the vortex shedding activity was visualized by fog generator, then captured by High Speed Photography. The smoke paths for a flow at Reynolds numbers of 80, 120 and 160 passing over the cylinder with a rotational speed α=6 is shown in Figure 4. It is evident how the stagnation point (encircled) has moved upwards based on Reynolds number.

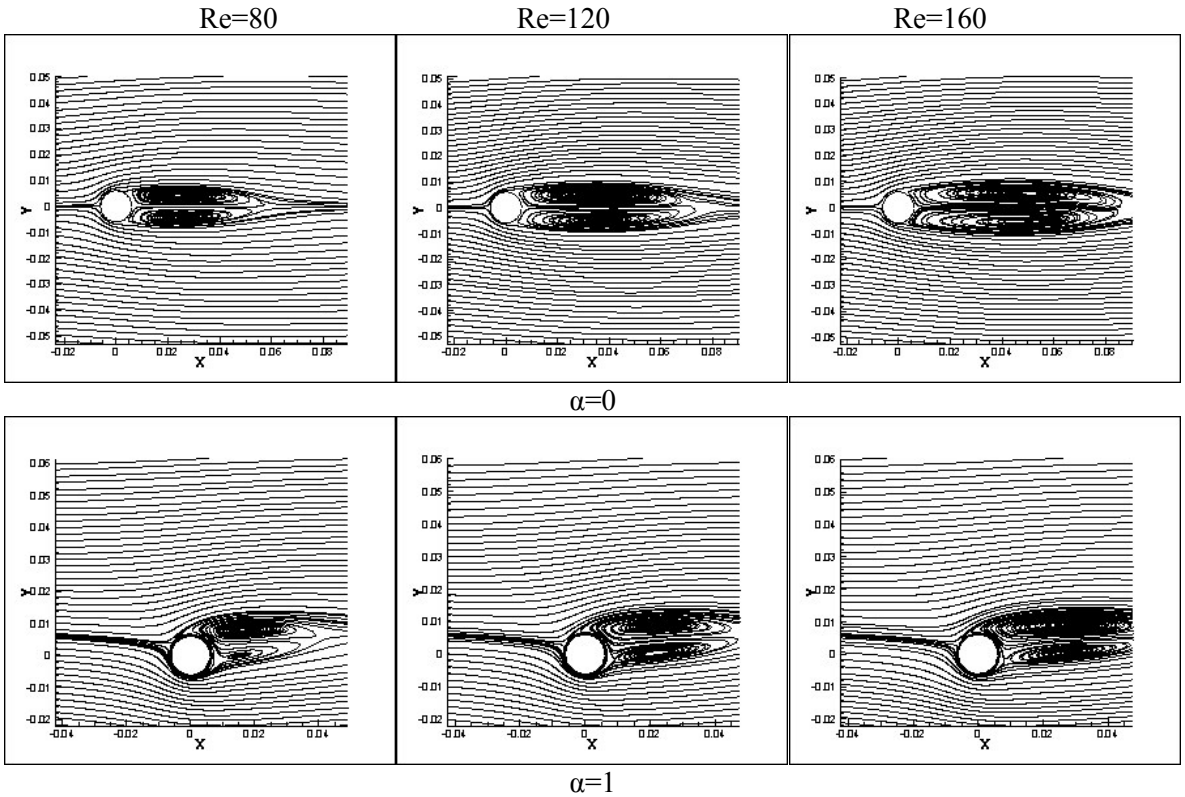

Figure 3. Continued

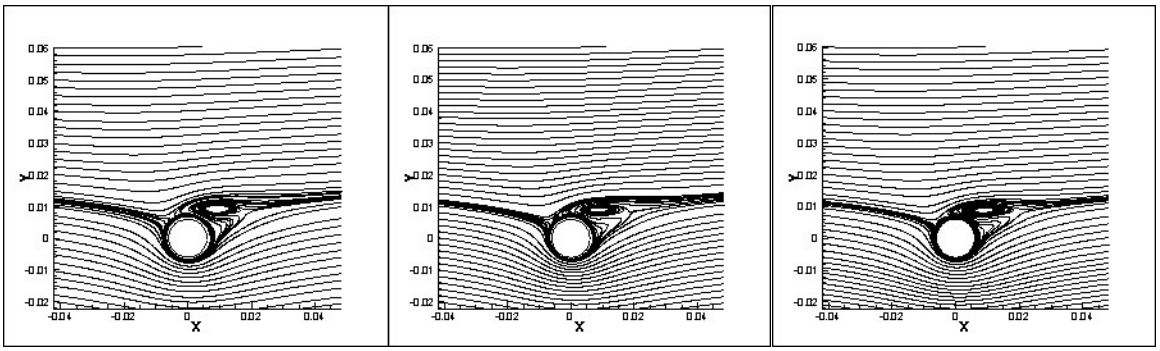

α=2

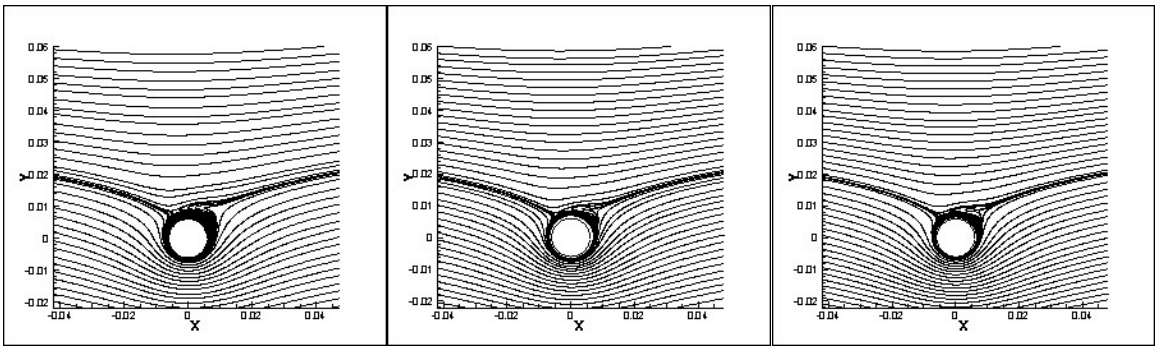

α=3

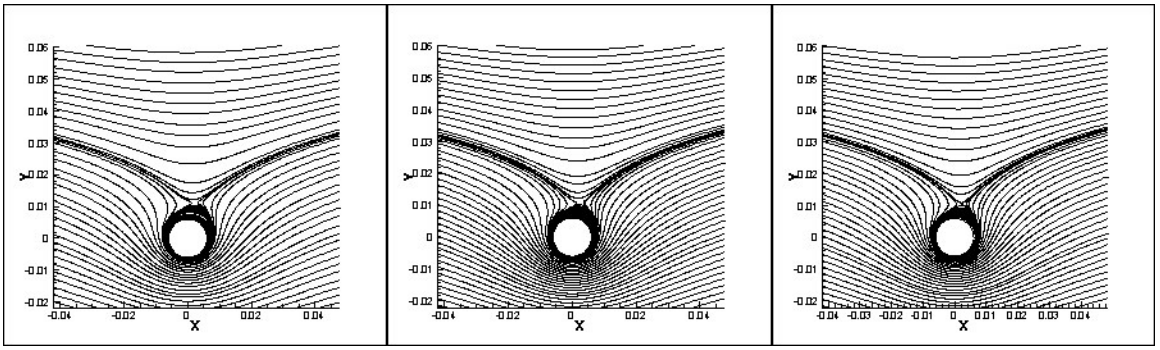

α=4

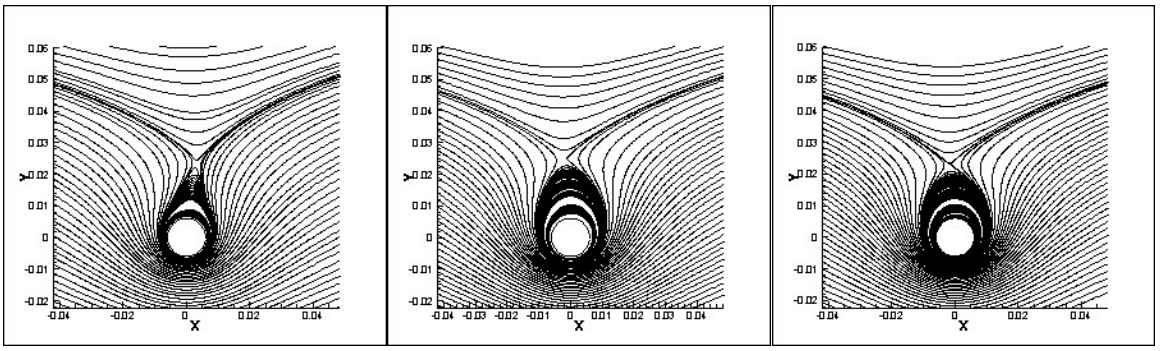

α=5

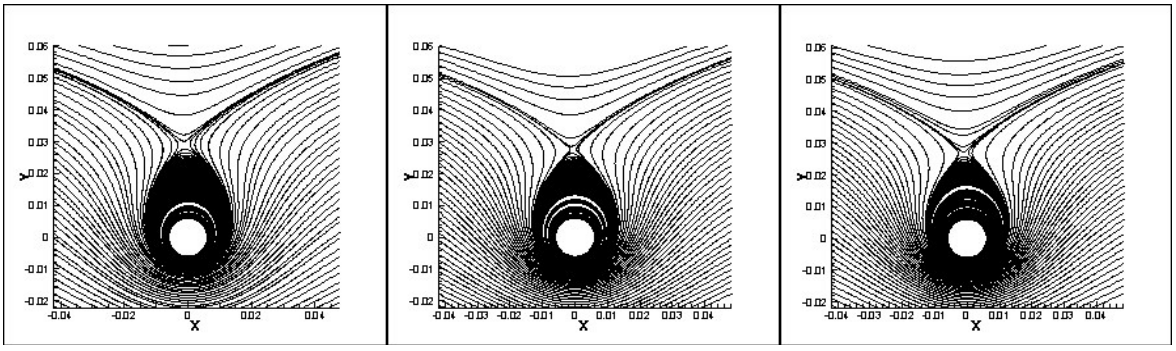

α=6

Figure 3. Streamlines for Re=80, 120 and 160, α= 0 - 6

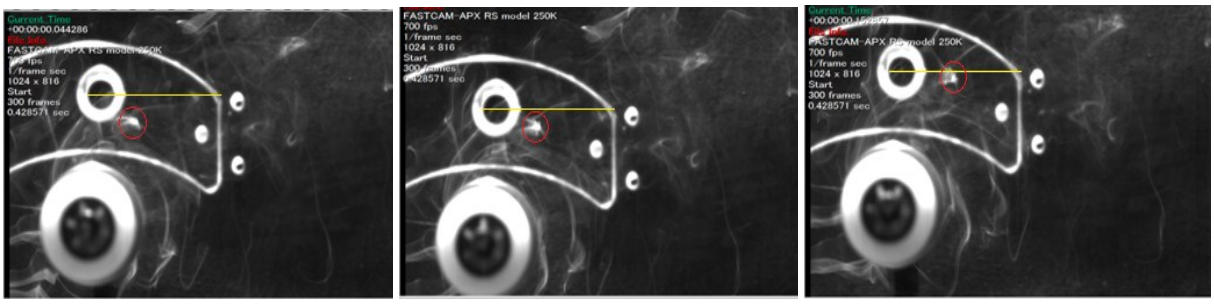

Figure 4. High Speed Photography at α=6 for Re = 80, 120 and 160

4.2 Velocity and pressure distributions

Figure 5 shows velocity distributions and pressure distributions in two dimensions for fluid flow around the stationary cylinder at the three values of inlet velocity 0.0975 m/s, 0.14625 m/s and 0.195 m/s at the inlet section which corresponding to Re=80,120 and 160 respectively. The general distributions of the velocity and pressure profiles are identical for all values of the velocities and as the inlet velocity increases, the velocity contour values increases. As the fluid approaches the stagnation point of the circular cylinder, it slows down and its pressure increases.

The smaller velocity within the boundary layer, leads to increase of the pressure. Thus, the induced pressure gradient causes a downward flow towards the cylinder surface, having impinged on the cylinder, the fluid rolls up forming vortices which finally warp around front half of cylinder and extended downstream of the separation point.

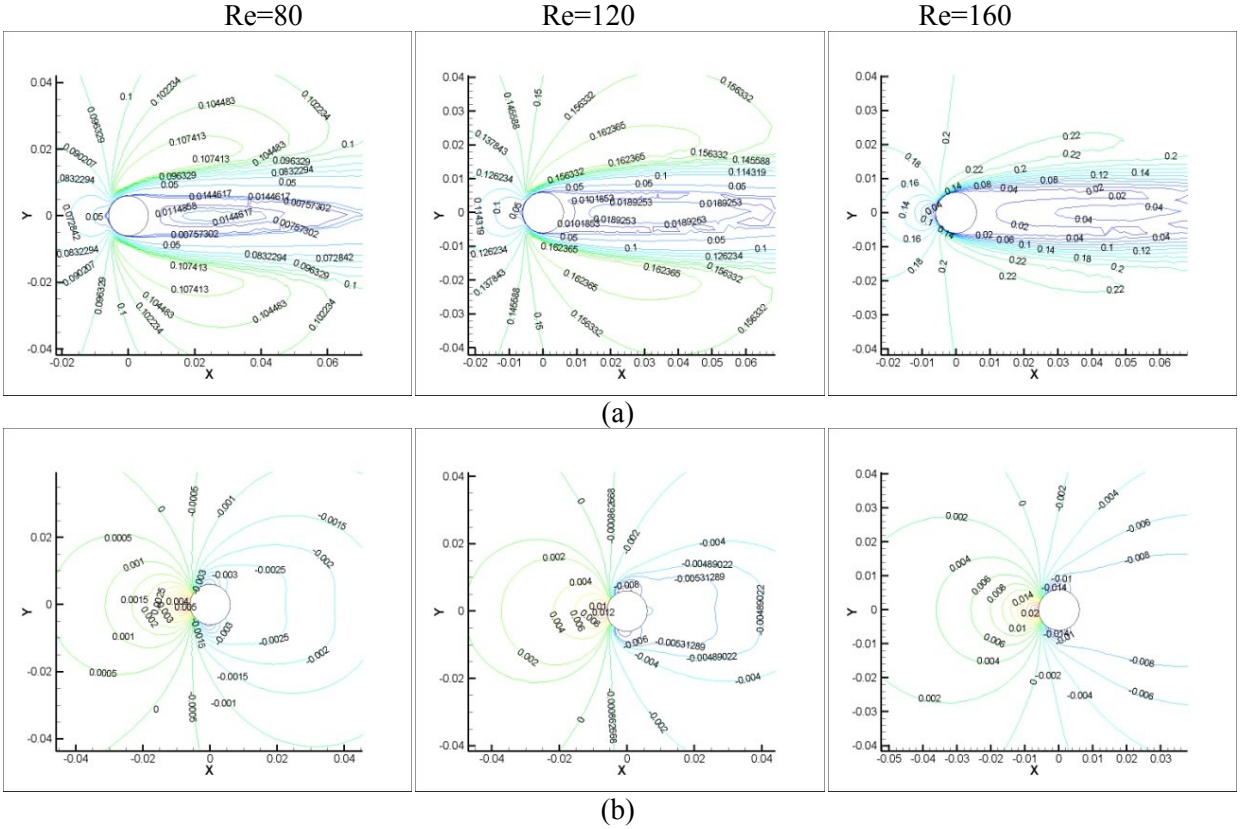

Figure 5. (a) velocity and (b) Pressure distributions for stationary cylinder

Figure 6 show the velocity distributions across the rotating cylinder with different rotational speed rate for α =1, 2, 3, 4, 5, and 6 respectively at Re=80,120 and 160 respectively. While Figure 7 shows the isobaric contours around the rotating cylinder with different rotational speed rate for α =1, 2, 3, 4, 5, and 6 at Re=80,120 and 160 respectively.

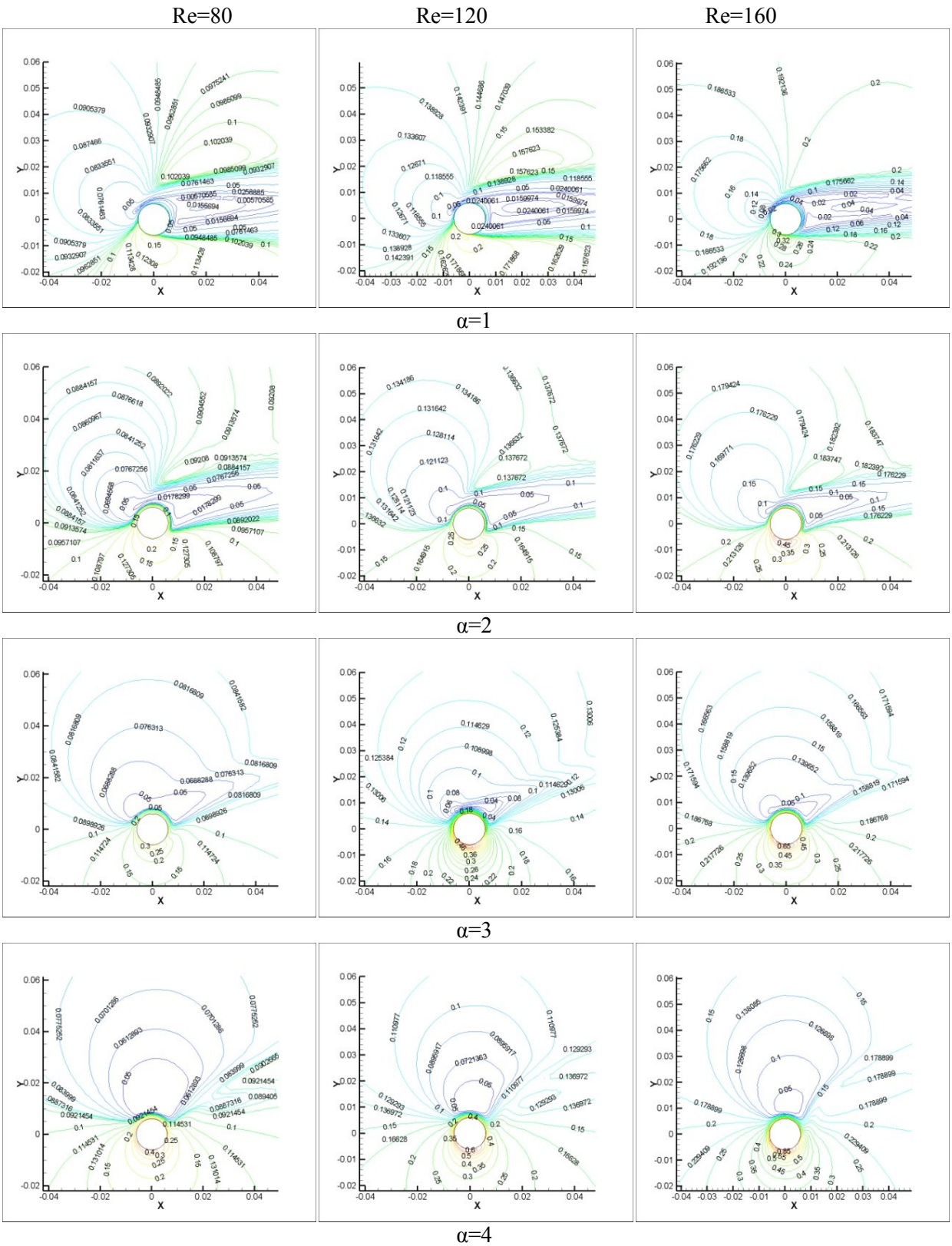

Figure 6. Continued

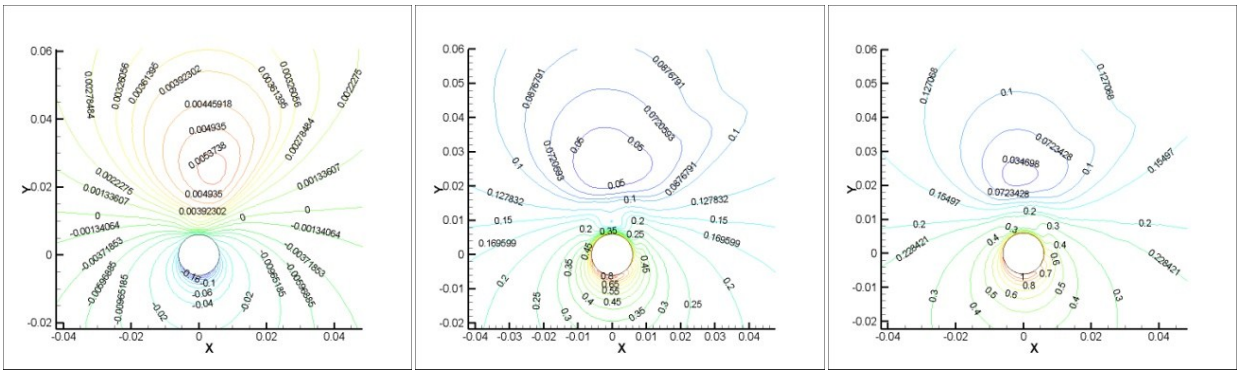

α=5

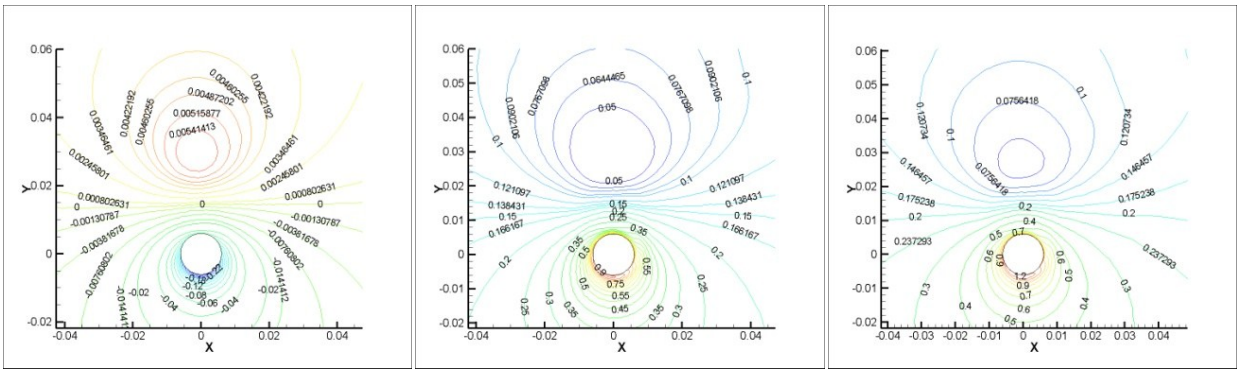

α=6

Figure 6. Velocity distributions for Re=80, 120 and 160, α= 0 - 6

Re=80 Re=120 Re=160

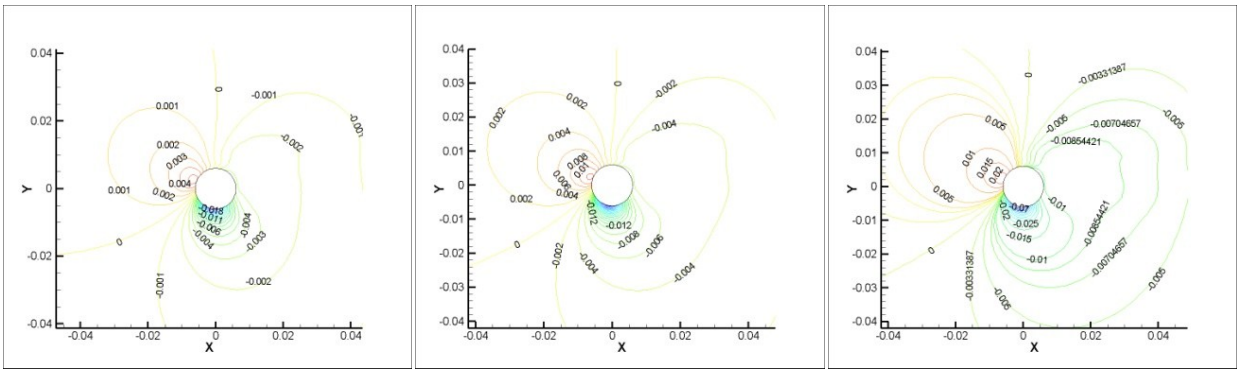

α=1

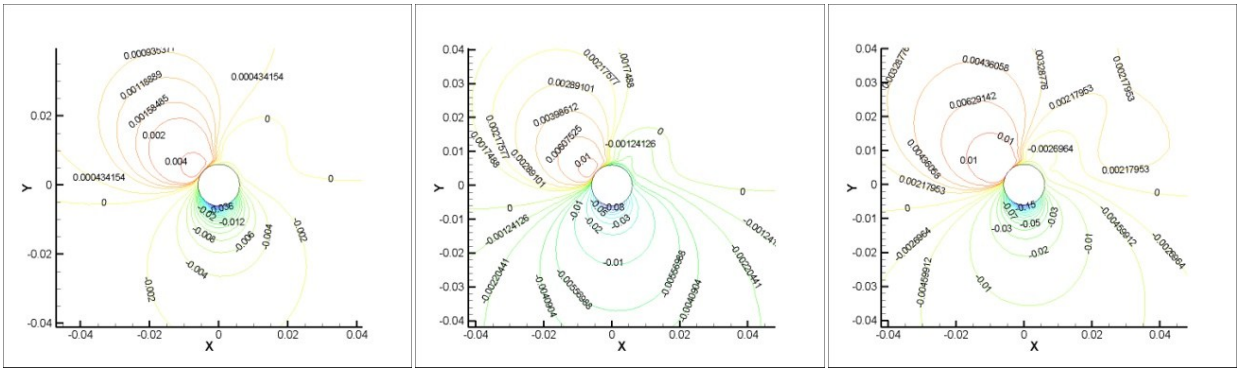

α=2

Figure 7. Continued

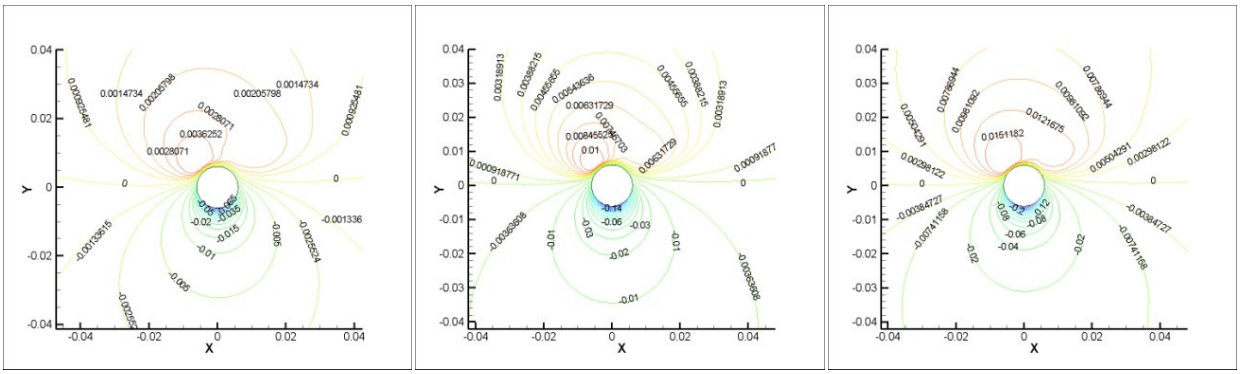

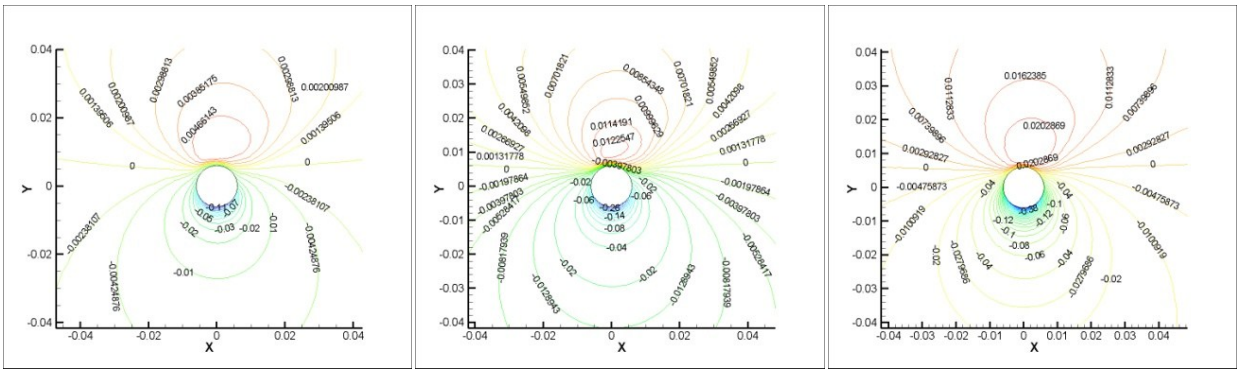

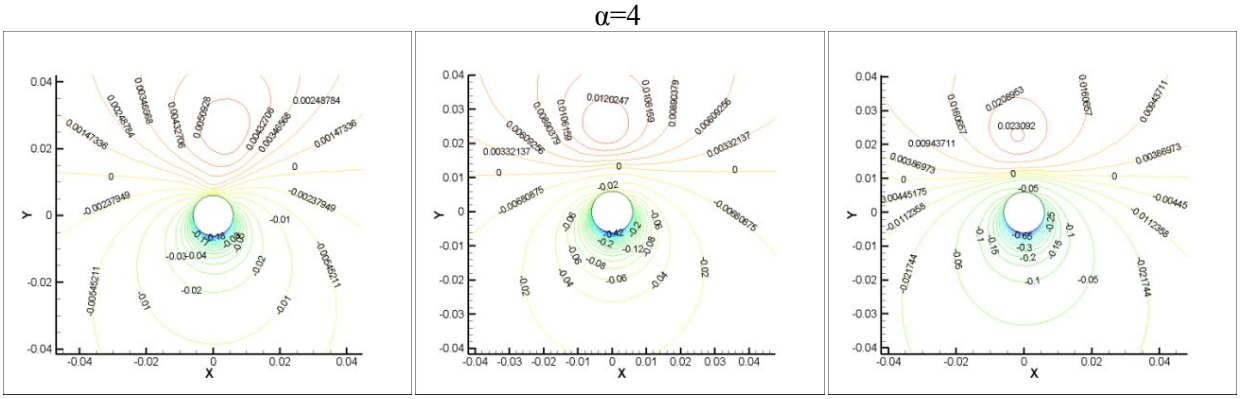

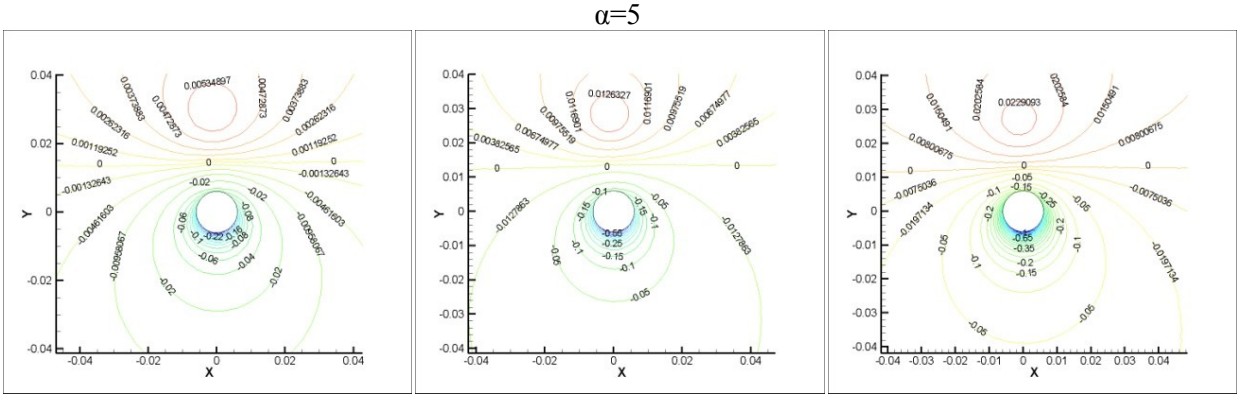

Figure 7. Pressure distributions for Re=80, 120 and 160, α= 0 - 6

It can be noted that the isobaric and velocity distributions are similar at the different values of Reynolds number for constant rotational speed but the values of incoming air speed increases with the increase of the air velocity and the velocity in the bottom side of the cylinder increase too while the velocity into the upper side was decreases as discuss previously.

At high rates of cylinder rotation, the pressure is negative along the entire streamlined contour. At the same time, the absolute values of pressure will near the upper one; so that the resultant force of pressure

forces is directed downward. The diagrams of velocity distribution on the cylinder boundary are qualitatively related. Near the lower side of the cylinder, on the opposite, the incoming and the rotational flow velocities are algebraically added, the fluid velocity decreases less intensively, and in some region inside the boundary layer it even exceed the rotation rate of α =6.
In Figure 8 (a) velocity diagram and (b) pressure forces along the cylinder contour at α=6 and Re=160 is given. The diagrams of velocity on the cylinder boundary are also qualitatively similar. Near the lower curve the rotational and the incoming flow velocities are added, the fluid velocity decreases less intensively. Art high rates of rotation the pressure is negative along the entire streamlined contour, the resultant force of pressure forces is directed downward.

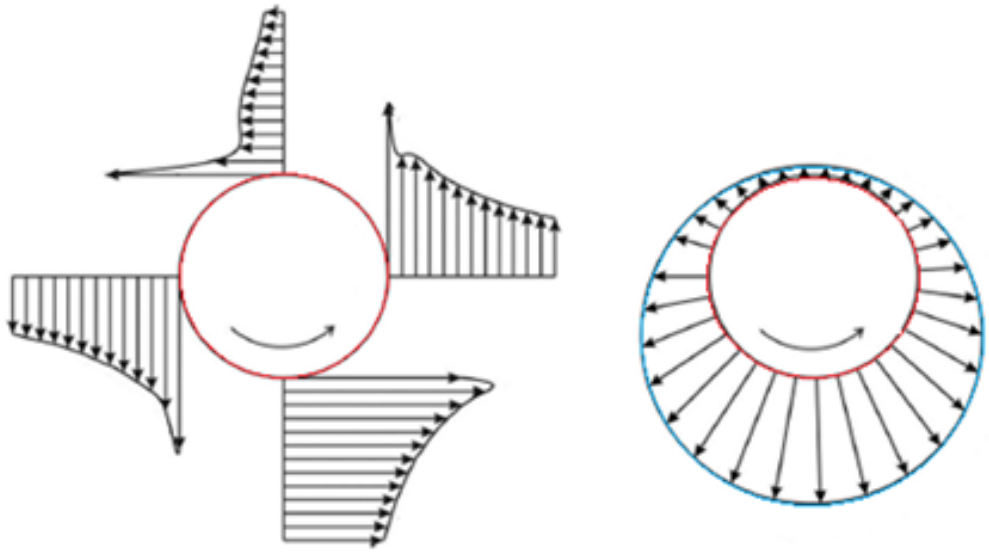

Figure 8. Distribution of (a) velocity diagram (b) pressure forces along cylinder contour at α=6 and Re=160

4.3 Mean lift and drag coefficient
Figures 9-11 are shown pressure coefficients cylinder along the angle from front side as in Figure 1(b). Pressure coefficient will increase for all rotational speed without contribute of Reynolds number. Maximum values of pressure coefficient are -47, -49 and -50 appears at (225-250) degree for α=6 for Re= 160, 120 and 80 respectively. Pressure coefficient values are convergent approximately and the maximum value at Re=80, this lead to vary in Re from 80 to 160 has small effect or not significant on pressure coefficient in same time value of rotation rate change from 1 to 6.

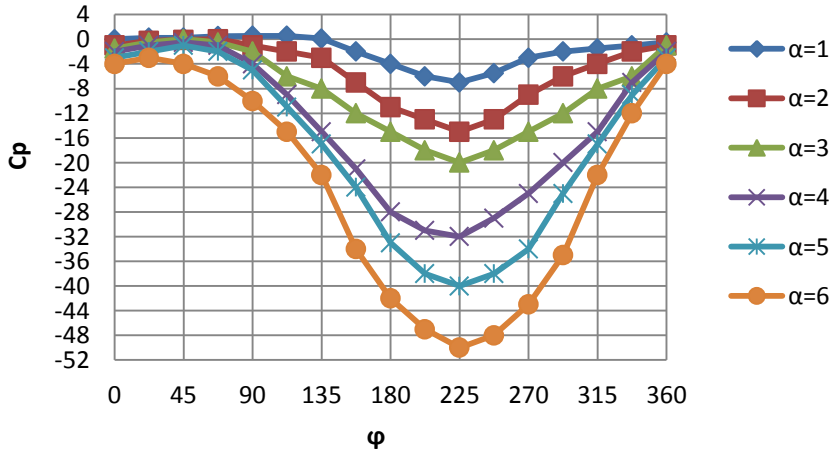

Figure 9. Pressure coefficient along angular position at Re=80

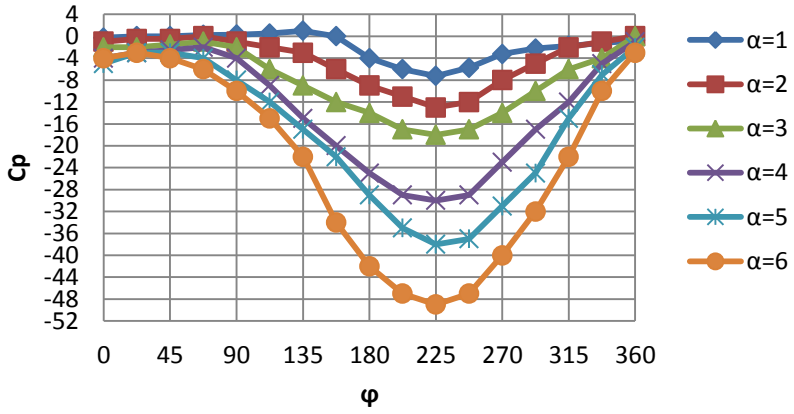

Figure 10. Pressure coefficient along angular position at Re=120

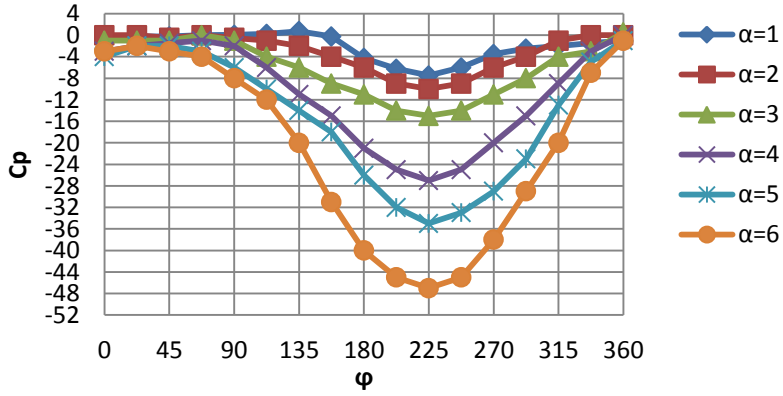

Figure 11. Pressure coefficient along angular position at Re=160

Figure 12(a) shows that the downward lift force, $C_L = C_{Lp} + C_{Lv}$, increases monotonically with increasing the rotation speed and with increasing Re. On the other hand, this increase is minor with increasing Reynolds number. So that, the lift coefficient is weakly dependent on Re and strongly dependent on rotation rate. Pressure force was found to effect more to total lift force as compared to viscous force. Figure 12 (b) shows the change of total drag coefficient, $C_D = C_{Dp} + C_{Dv}$, with rotation speed rate a for all Re. For the stationary cylinder, the pressure drags effect more to total drag. On the other hand, for rotating cylinder, the contribution of viscous drag increases stridently with increase of rotational speed and be more than that of pressure drag at the largest rotational speed. With increase the rotational speed, C_D decreases gradually until the rotation rate reach 4 and then it increases when an increasing movement of viscous drag dominates over the decreasing movement of pressure drag.

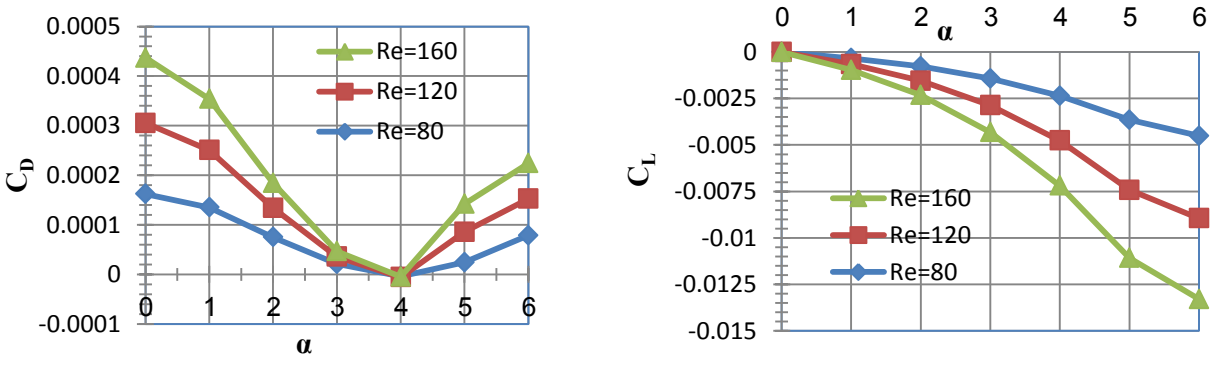

(a) (b)

Figure 12. Variation of (a) Total lift coefficient (b) Total drag coefficient with rotation rate α for various Re

4.4 Turbulence intensity

In the present work, the turbulence intensity was calculated to examine the effect of cylinder rotation on vortex formation. Figures 13-15 shows the experimental results of turbulence intensity using LDV under various conditions at Re=80,120 and 160 for stationary and rotating cylinder (α=0, 2,4,6). It can be noted that the values are less than 1% as the low average air speed passing over the cylinder. The positions of the selected points are on top of the cylinder and point 4 is directly above the center of the cylinder.

Generally, the turbulence intensity increases with the Reynolds number for all cases as the kinetic energy increases. For the stationary cylinder (α=0), the figures show that the turbulence intensity is small ahead the cylinder and start to increase because of the twin vortex at the back of cylinder. The effect of rotation appears clearly in the figures and the turbulence intensity is shifted with increase the rotational speeds of the cylinder. The turbulence intensity has significant effects at the high rotational speed (α=6).

Theoretical results for turbulence intensity are compared with the experimental results in Figure 16 at α=6 for Re=80,120 and 160. A good agreement is obtained with maximum errors 12.6% so that the theoretical results also show that the cylinder rotation reduces the fluctuation in the region next to the cylinder as shown in the Figure 17. Due to the rotation of the cylinder, the rotating flow intersects the upstream flow developing a zone of high turbulence before the cylinder, whilst the flow remains smoother near the cylinder. The streamlines in [11] and [19] support the explanation.

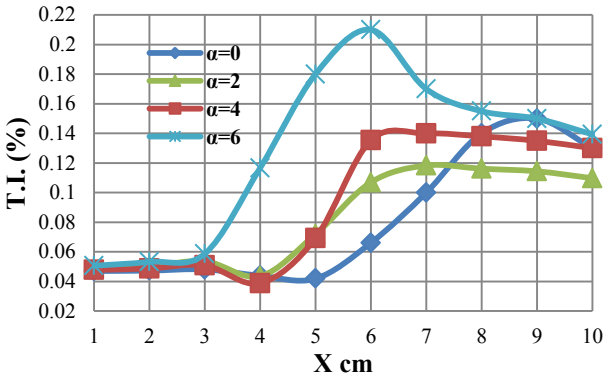

Figure 13. Turbulence intensity for α=0,2,4,6 at Re=80

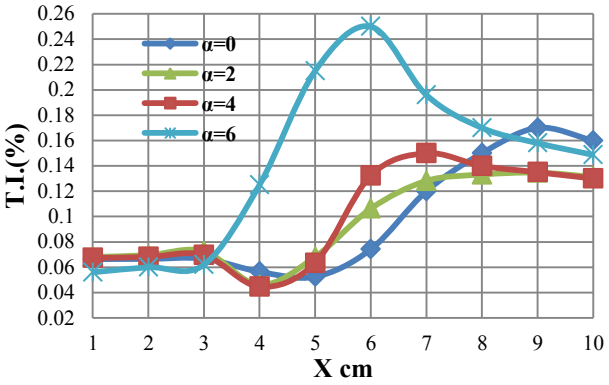

Figure 14. Turbulence intensity for α=0,2,4,6 at Re=120

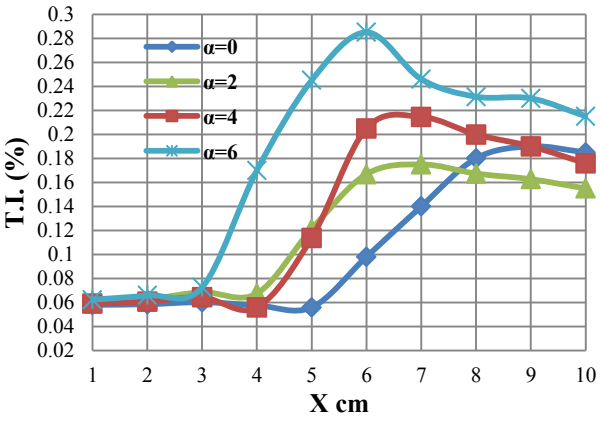

Figure 15. Turbulence intensity for α=0,2,4,6 at Re=160

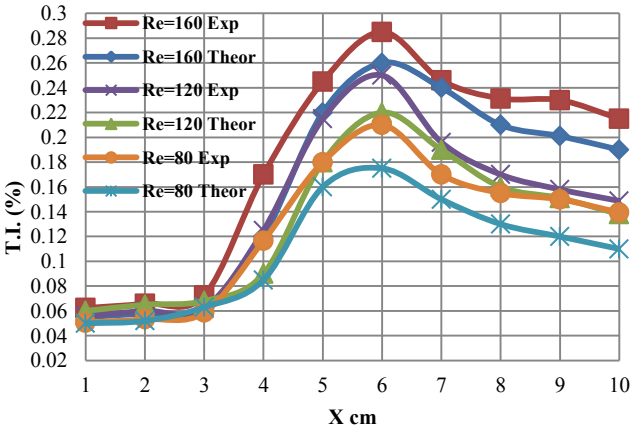

Figure 16. Experimental and theoretical results for α=6 at Re=80,120,160

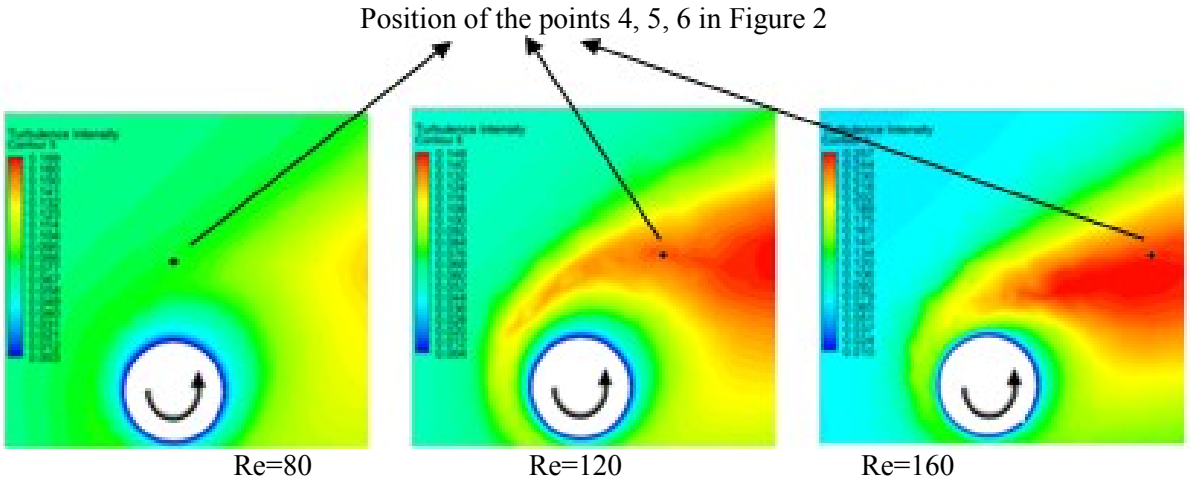

Figure 17. Turbulence intensity close to cylinder for α=6 at Re=80,120,160.

5. Conclusion

Fluid flow passing around a stationary and rotating circular cylinder with uniform flow of Re = 80, 120 and 160 has been studied experimentally and numerically for various rotation rates α = 0, 1, 2, 3, 4, 5 and 6. The work was achieved using flow visualization techniques that include High Speed Photography and LDV techniques. It was found that at higher α, the turbulence decreases downstream the cylinder, with a high peak just upstream as a consequence of the clashing flows. It can be conclude that the lift coefficient increases with increase the rotation rate and effect of Reynolds number small effect on lift coefficient. Also it can be conclude as rotation rate increase, the pressure coefficient will increase too and the variation in Reynolds number from 80 to 160 has small effect or not significant on pressure coefficient. Downward lift force is found increases monotonically with increase the rotational speed and remain almost constant with increasing Re. So that the rotation can be used as a drag reduction technique as the drag coefficient reduces monotonically with increase the rotational speed up to 4 with a value close to zero at α = 4 for all Re. However, generally increase values of skin friction coefficient with increase of rotation rate. Comparisons of the numerical and experimental results with other published works give a good agreement.

Acknowledges

The authors would like to take the opportunity to thank EPSRC Pool of Instruments for their contributions to the results obtained. The help of Mr. Martin Hyde from TSI and the machinist Mr. Malcolm Seabourne in fabricating some of the experimental components into Cardiff University is also gratefully acknowledge. Finally, the authors gratefully acknowledge the Iraqi Government (MOHESR) for its support.

Nomenclature

C_D	Total drag coefficient (=C_{Dp} + C_{Dv})	F_{Lv}	Viscous lift force on the cylinder
C_{Dp}	Pressure drag coefficient (=F_{Dp} /$0.5\rho\, u_\infty{}^2 D$)	L	Lift force (N)
C_{Dv}	Viscous drag coefficient (=F_{Dv} /$0.5\rho\, u_\infty{}^2 D$)	p	Local pressure (N/m2)
C_f	Skin friction coefficient	P_∞	Pressure as coordinate goes to infinity (N/m2)
C_L	Total Lift coefficient (=C_{Lp} + C_{Lv})	r	Radius in polar coordinate
C_{Lp}	Pressure lift coefficient (=F_{Lp} /$0.5\rho\, u_\infty{}^2 D$)	R	Radius of the cylinder
C_{Lv}	Viscous lift coefficient (=F_{Lv} /$0.5\rho\, u_\infty{}^2 D$)	Re	Reynolds number
C_p	Pressure coefficient	u, v, w	Velocity component in x, y, z - direction respectively (m/s)
D	Diameter of the cylinder	U_∞	Free velocity of fluid (m/s)

F_{Dp}	Pressure drag force on the cylinder	x , y, z	Cartesian coordinate in horizontal, vertical, depth direction (m)
F_{Dv}	Viscous drag force on the cylinder	α	Non-dimensional rotational velocity=ω D/2u∞
F_{Lp}	Pressure lift force on the cylinder	ϕ	Angular displacement
		ω	Angular velocity of cylinder rotation, rads¯1

References

[1] Prandtl, L., The Magnus effect and wind-poered ships, Naturwissenschaften, vol.12 pp. 93-108, 1925.

[2] Choutanceau, M. and Menard, C., Influence of rotation on the near-wake development behind an impulsively started circular cylinder, J. Fluid Mech., vol. 158, pp. 399-446, 1985.

[3] Lam, K. M., Vortex shedding flow behind a slowly rotating circular cylinder, J.Fluids Struct., vol. 25, pp. 245-262, 2009.

[4] Chew, Y. T., Cheng, M., and Luo, S. C., 1995, "A Numerical Study of Flow Past a Rotating Circular Cylinder Using a Hybrid Vortex Scheme," J. Fluid Mech., 299, pp. 35-71.

[5] Kang, S., Choi, H., and Lee, S., Laminar flow past a rotating circular cylinder, Phys. Fluids, vol. 11, no. 11, pp. 3312 - 3321, 1999.

[6] Stojkovic, D., Breuer, M., and Durst, F., Effect of high rotation rates on the laminar flow around a circular cylinder, Phys. Fluids, Vol. 14, No. 9, pp. 3160-3178, 2002.

[7] Mittal, S. and Kumar, B., Flow past a rotating cylinder, J. Fluid Mech., vol. 476, p. 303-334, 2003.

[8] Mazo, A. B. and Morenko, I. .V., Numerical simulation of a viscous separation flow around a rotating circular cylinder, J. Eng. Thermophys., vol. 79, no. 3, pp. 496-502, 2006.

[9] Prihod'ko, A. A. and Redtchits, D. A., Numerical modeling of a viscous incompressible unsteady separated flow past a rotating cylinder, Fluid Dyn., vol. 14, no. 6, pp. 823-829, 2009.

[10] Badr, H. M., and Dennis, S. C. R., 1985, "Time-Dependent Viscous Flow Past an Impulsively Started Rotating and Translating Circular Cylinder," J. Fluid Mech., 158, pp. 447-488.

[11] D. B, Ingham and T. Tang, "A Numerical Investigation into the Steady Flow Past a Rotating Circular Cylinder at Low and Intermediate Reynolds Numbers", Reprinted from Journal Of Computational Physics Vol. 87, No.1, New York and London, March 1990.

[12] S. Kumar, C. Cantu and B. Gonzalez, Flow Past a Rotating Cylinder at Low and High Rotation Rates , Journal of Fluids Engineering, April 2011, Vol. 133

[13] Ressan Faris Al-Maliky Numerical Investigation of Laminar Flow over a Rotating Circular Cylinder , International Journal of Mechanical & Mechatronics Engineering IJMME-IJENS Vol:13,No:03, pp: 32-44, 2013

[14] T. Ayyappan and S. Vengadesan, Influence of Staggering Angle of a Rotating Rod on Flow Past a Circular Cylinder , Journal of Fluids Engineering, MARCH 2008, Vol. 130

[15] Jan O. Pralits, Flavio Giannetti and Luca Brandt, Three-dimensional instability of the flow around a rotating circular cylinder , J. Fluid Mech.,vol. 730, pp. 5-18.,2013

[16] Engelman, S. M., and Jamnia, M. A., "Transient Flow Past a Circular Cylinder: A Bench Mark Solution," Int. J. Numer. Methods Fluids, 11, pp. 985-1000, 1990.

[17] Meneghini, J. R., Saltara, F., Siqueria, C. L. R., and Ferrari, J. A., "Numerical Simulation of Flow Interference Between Two Circular Cylinders in Tandem and Side-By-Side Arrangements," J. Fluids Struct., 17, pp. 561–577, 2001.

[18] Oula M.H. Fatla, Ghassan F. Smaisim, Agustin Valera-Medina, A.M. Rageb , N. Syred, Experimental and Numerical Investigation of Heat Transfer and Fluid Mechanics across a Rotating Circular Cylinder Dissipating Uniform Heat Flux by Crossflow, 10th Pacific Symposium on Flow Visualization and Image Processing Naples, Italy, 15-18 June, 2015. www.psfvip10.unina.it/Ebook/web/papers/ 045_PSFVIP10.pdf

[19] H.M. Badr, S.C.R. Dennis and P.J.S Young, Steady And Unsteady Flow Past A Rotating Circular Cylinder At Low Reynolds Numbers , Computers and fluids, Vol. (17) ,No.4, pp. 579-609, 1989.

